Journal of Tropical Resources and Sustainable Science
Website : http://journal.umk.edu.my/index.php/jtrss/
eISSN : 2462-2389
Vol: 14, Issue 2, 2026, 288-296
DOI: https://doi.org/10.47253/jtrss.v14i2.1902

RESEARCH ARTICLE

Application of TIG-MIG hybrid welding for wire arc additive manufacturing

Rey Kar Seah[1], Nur Ain Atiqah Jamaluddin[1], Syahril Azli Abdul Rahman[1], Sarizam Mamat[1]*, Mohd Fadzil Abdul Kadir[2], Ahmad Nazri Dagang[3], Mohamad Shaiful Ashrul Ishak[4] and Toshifumi Yuji[5]

[1]Faculty of Bioengineering and Technology, Universiti Malaysia Kelantan, Jeli Campus, 17600 Jeli, Kelantan, Malaysia.
[2]Faculty of Informatics and Computing, Universiti Sultan Zainal Abidin, Besut Campus, Besut 22200, Terengganu, Malaysia.
[3]Faculty of Ocean Engineering Technology, Universiti Malaysia Terengganu, 21030 Kuala Nerus, Terengganu, Malaysia.
[4]Faculty of Mechanical Engineering & Technology, Universiti Malaysia Perlis, Pauh Putra Campus, 02600 Arau, Perlis, Malaysia.
[5]Faculty of Education, University of Miyazaki, 1-1 Gakuenkibanadai-Nishi, Miyazaki 889-2192, Japan.

ARTICLE HISTORY
Received : 9 November 2025
Accepted : 28 January 2026
Online : 30 June 2026

KEYWORDS
Wire Arc Additive Manufacturing,
TIG-MIG hybrid,
MIG,
Heat input,
Heat accumulation,
Microhardness

☒ * **CORRESPONDING AUTHOR**
Assoc. Prof. Ts. Dr. Sarizam Mamat
Faculty of Bioengineering and Technology, Universiti Malaysia Kelantan, Jeli Campus, 17600 Jeli, Kelantan, Malaysia
Email: sarizam@umk.edu.my

ABSTRACT

Wire arc additive manufacturing (WAAM) is an advanced 3D printing technology that fabricates metal components through layer-by-layer deposition using an electric arc as the heat source. However, excessive heat input during repeated thermal cycles in WAAM leads to microstructural coarsening, grain growth and phase instability, which adversely affect mechanical properties. This research aims to apply TIG-MIG hybrid welding in WAAM and compare its performance with conventional MIG welding. The methodology involved depositing four successive welding layers using both TIG-MIG hybrid and MIG processes. The parameters including, current (A), voltage (V), torch configuration, welding speed and wire feeding rate are investigated. The welds are characterized using optical microscopy to observe microstructura; changes and microhardness testing to evaluate the mechanical properties. Results showed that the TIG-MIG hybrid reduced heat input by 7.41% (from 621.00J/mm to 575.00 J/mm) across four layers, with surface temperature decreased from 195.4 ℃ to 231.4 ℃. The hybrid process produced nearly twice the reinforcement height (from 2.286 mm to 6.304 mm) compared to MIG, while the penetration depth decreased from 1.281 mm to 0.816 mm. Microstructural analysis revealed refined ferritic dendrite structures in TIG-MIG hybrid welds compared to the coarser dendrites observed in MIG. Although the TIG-MIG hybrid exhibited slightly lower hardness values (129.9 HV-221.57 HV) compared to MIG (168.17 HV-245.17 HV, the refined microstructure suggests improved toughness and mechanical ability. Overall, TIG-MIG hybrid welding in WAAM effectively mitigates excessive heat input, enhances bead geometry, and refines microstructure compared to MIG, making it a promising approach for improving the mechanical performance of multilayer WAAM components.

1. INTRODUCTION

Additive manufacturing (AM), commonly known as 3D printing or rapid prototyping, is a layer-by-layer fabrication method that reduces material waste, production time and overall costs through digitally controlled processes (Karayel & Bozkurt, 2020). AM is widely applied in various industries including biomedical, aerospace, and automotive sectors (Jafari et al., 2021; Jamian et al., 2018; Singh et al., 2020). Metal AM processes are generally classified into four categories such as powder bed fusion (PBF), direct energy deposition (DED), binder jetting and sheet lamination (Zhang et al., 2018).

Wire arc additive manufacturing (WAAM) is a DED process that utilizes wire feedstock and electric arc welding tools as the energy source to build components from deposited weld material (Ding et al., 2015). Various electric arc welding processes can be employed in WAAM, including gas metal arc welding (GMAW), gas tungsten arc welding (GTAW) and plasma arc welding (PAW) (Dinovitzer et al., 2019).

WAAM offers several advantages, such as low manufacturing cost, reduce carbon footprint, shorter production time, and the capability to fabricate large-scale components (Ding et al., 2015). However, excessive heat input often leads to residual stresses, poor surface quality, high heat accumulation, and inconsistent weld bead geometry (Dinovitzer et al., 2019). Therefore, several studies have investigated the optimization of process parameters to control heat input, which significantly influences the microstructure of welded components in WAAM (Oliveira et al., 2020).

MIG-based techniques have been extensively investigated for WAAM manufacturing. Although MIG-based techniques offer high efficiency and relatively low capital cost, they are not always recommended due to challenges associated with WAAM processing. These challenges include residual stresses and distortion caused by excessive heat input, leading to poor surface quality (Shah et al., 2023), as well as non-uniform weld transitions and geometries, which hinder dimensional accuracy and mechanical performance (Bach et al., 2025; Karayel & Bozkurt, 2020). Rodrigues et al. (2019) reported that excessive heat accumulation during WAAM manufacturing hinders accurate control of weld bead geometry, resulting in residual stresses that influence microstructure formation and mechanical properties. Yang et al. (2017) reported that GMAW-based technique provide a high deposition rate in WAAM but are prone to high heat accumulation as the deposition layer increases, leading to residual stress in the final component. Snopiński et al. (2018) demonstrated that residual stress and distortion are among the most significant challenges in WAAM due to high heat input, which promotes columnar microstructure formation, and reduces mechanical performance, particularly under brittle fracture conditions. Consequently, optimizing WAAM parameters by reducing the welding current or increasing the travel speed helps control heat input, which may result in approximately 7.41% reduction (from 621 J/mm to 575 J/mm), thereby reducing melt volume per deposition layer. This enhances microstructural refinement and improves ductility and toughness of the final component (Dinovitzer et al., 2019).

Hybrid welding technologies in WAAM, including TIG-MIG, laser-arc, and double-electrode GMAW systems, have shown significant progress in overcoming the limitations of conventional processes. These approaches improve arc stability, reduce spatter, and lower heat input, resulting in refined ferritic dendrite structures and improves bead geometry with higher reinforcement and reduced penetration (He et al., 2025; Kapil et al., 2022). For instance, TIG-MIG hybrid demonstrated a reduction in molten pool volume by approximately 30%, mitigating heat accumulation and producing finer microstructures with improved mechanical performance in WAAM (Yang et al., 2016). Yang et al. (2016) further demonstrated a similar concept through a double electrode GMAW system with a TIG bypass arc, which stabilized the molten pool. The TIG-MIG hybrid process improved microstructural refinement with no prominent coarsening as compared to conventional GMAW, due to a lower temperature gradient in the weld pool with appropriate adjustment of welding parameters (Liberini et al., 2017). In this research, the TIG-MIG hybrid welding technique is introduced by combining the arc stability of TIG with the high deposition rate of MIG in WAAM. The study focuses on spatter formation, welding current, heat input, surface temperature, weld bead geometry, microstructure, and mechanical properties in comparison with conventional MIG welding. The findings aim to demonstrate improvements in toughness, ductility, spatter reduction, and deposition efficiency, thereby making hybrid welding as a promising approach for advancing WAAM applications.

2. EXPERIMENTAL SETUP

The schematic diagram of the TIG-MIG hybrid experimental setup is shown in Figure 1. A D-STEP “THK Robo Cylinder” (purchased from THK Co., Ltd.) programmable linear actuator was employed to precisely control the motion of the workpiece during automated welding. The actuator controlled the movement of the work platform for two experimental groups, TIG-MIG hybrid welding and MIG welding during WAAM fabrication. In the TIG-MIG hybrid welding configuration, the TIG torch was placed in the leading direction while, the MIG torch was placed in the trailing direction to enhance arc stability during the deposition process. In this work, the Riland MIG300GD welding machine was served as the MIG power supply while, Riland TIG 315P AC/DC was used as the TIG power source. During deposition, both TIG and MIG torches were maintained in fixed positions, and the workpiece was mounted on a movable platform translated from right to left to enable layer-by-layer deposition in WAAM. This setup ensured the welding direction was controlled by the movement of workpiece rather than by torch motion.

WAAM deposition was performed on S50C medium carbon steel substrate plate (150 mm × 50 mm × 6 mm) using ER70S-6 mild steel wire filler with a diameter of 1.0 mm. Pure argon (Ar) was used as the shielding gas at constant flow rates of 10 L/min for TIG and 15 L/min for MIG. The welding speed and wire feed rate were set to 36 cm/min and 6.8 m/min respectively, to balance deposition efficiency with bead geometry control. The angle of TIG-MIG hybrid in TIG-15°/MIG+18° was applied and other parameters were selected based on preliminary trials. The MIG current (180 A) was employed to achieve efficient deposition, while the TIG current (100 A) was kept lower to stabilize the arc and reduce heat input. Voltage was maintained between 19 V and 23 V to ensure consistent arc length as listed in Table 1. Surface temperature during deposition was measured using an infrared thermometer at both arc striking and arc extinguishing points (Figure 2). Surface temperature of heat accumulation were measured after welding and 5 minutes afterwards of interlayer cooling. In addition, the current changes of the power supply were observed for both TIG-MIG hybrid and MIG

welding. For the hybrid configuration, the current was continuously recorded using a digital data acquisition system connected to the welding power source. Prior to experiment, the measuring unit was calibrated against a standard reference meter to ensure accuracy. Heat input was calculated using Equation 2.1:

$$H = \frac{VI}{v} \qquad \text{Equation 2.1}$$

Where;

H is heat input in J/mm;
V is voltage in V;
I is current in A;
v is welding speed in mm/s.

For metallographic analysis, specimens were sectioned from the deposited weld beads at a thickness of 10mm at the centre of each specimen (Figure 3). The specimens were subsequently polished to a mirror-surface for microstructural observation. Each specimen was etched either using 3wt.% Nital for 20 seconds or by using LePera solution within different etching durations (50 seconds, 40 seconds and 30 seconds), followed by oscillation. The location of microstructure was analysed by using optical microscope (Meiji Techno Model IM7530) using these two etchants of 3wt.% Nital and LePera solution, respectively (Figure 4). Microhardness test was conducted by using Vickers's microhardness machine (Mitutoyo HM-210/220 Vickers Hardness Testing Machine) with a load of 0.1N at 10 seconds dwell times. All specimens were cut (30mm x 6mm x 6mm) according to the ASTM E92. All measurements of weld bead geometry including, weld bead width, reinforcement height and depth penetration for TIG-MIG hybrid and MIG of WAAM were measured using an open source, imaging software, ImageJ version 1.54g.

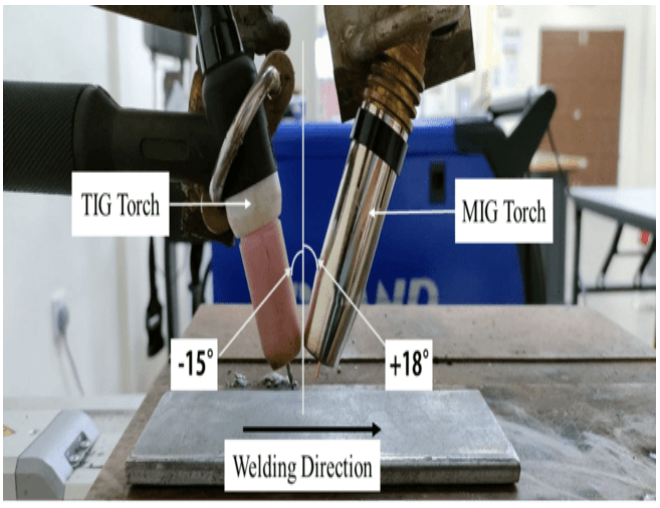

Figure 1: The schematic diagram of TIG-MIG hybrid of experimental set up

Table 1: Experimental parameter of TIG-MIG hybrid and MIG based WAAM.

Condition	Parameters	
Welding Torch	TIG	MIG
Polarity	DCEN	DCEP
Filler Wire	ER70S-6 Ø 1.0 mm	
Current (A)	100	180
Voltage (V)	19	23
Contact Tip Work Distance (mm)	-	17
Tungsten Tip to Workpiece Distance (mm)	10	-
Torch Angle (TIG/MIG)	TIG -15°/MIG+18°	
Distance between TIG and MIG electrodes (mm)	9	
Welding Speed (cm/min)	36	
Shielding gas	Argon (Ar)	
Shielding gas flow (L/min)	10	15
Wire Feed Rate (m/min)	6.8	
Deposited Length (mm)	80	
Interlayer Cooling Rate (min)	5	
Total Number of Layers	4	

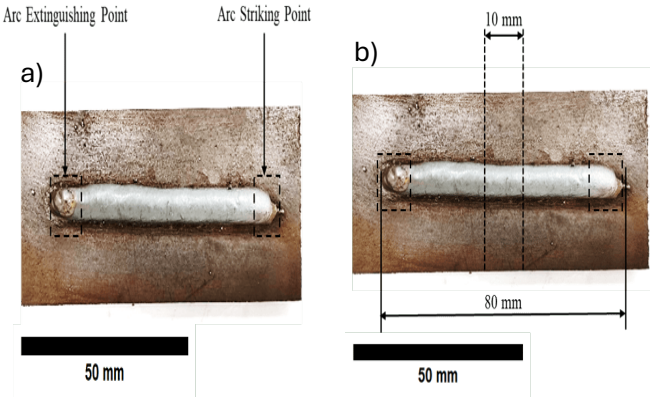

Figure 2: The schematic diagram of (a) thermal analysis position for WAAM and (b) cross-sectional cut area.

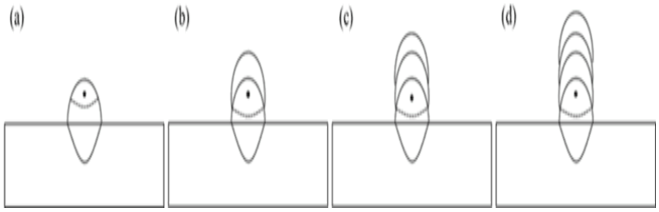

Figure 3: The microstructure observation area of WAAM in TIG-MIG hybrid and MIG. (a) 1 layer; (b) 2 layers; (c) 3 layers; (d) 4 layers. The black dot represents the fixed observation area on the deposited weld bead. This location was kept constant across all layers to ensure consistency in microstructural comparison.

3. RESULT AND DISCUSSION

3.1. Effect of welding current and heat input for WAAM

Welding current and heat input effects of the TIG-MIG hybrid and MIG of WAAM are presented in Figure 4 and Figure 5, respectively. Under identical parameters, including filler wire used, wire feed rate and welding speed, the TIG-MIG hybrid consistently exhibited lower welding current and heat input compared to MIG. The welding current in the TIG-MIG hybrid process decreased by 7.4% (from 162 A to 150 A) as

the number of layers increased from the 1st to the 4th layer. In comparison, MIG welding current decreased by 11% (from 198 A to 176 A). Similarly, the heat input of TIG-MIG hybrid welding decreased from 621.00 J/mm to 575.00 J/mm, while MIG decreased from 759.00 J/mm to 674.67 J/mm. These results indicate the TIG-MIG hybrid process effectively reduces heat input into the base metal through the auxiliary TIG arc, contributing to improved thermal control during deposition (Rodrigues et al., 2019).

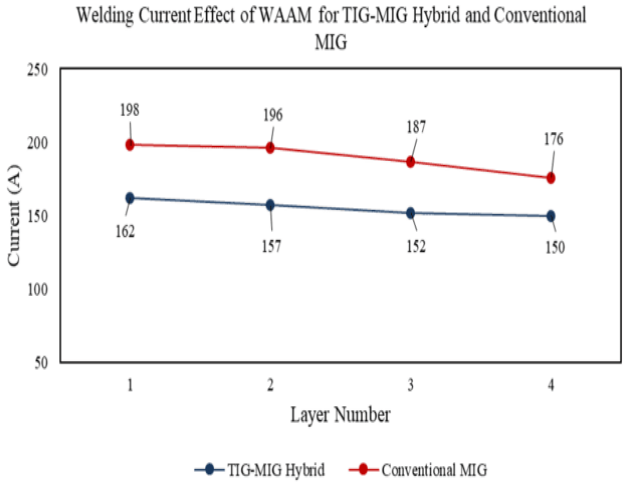

Figure 4: The welding current effect of WAAM for TIG-MIG Hybrid and MIG.

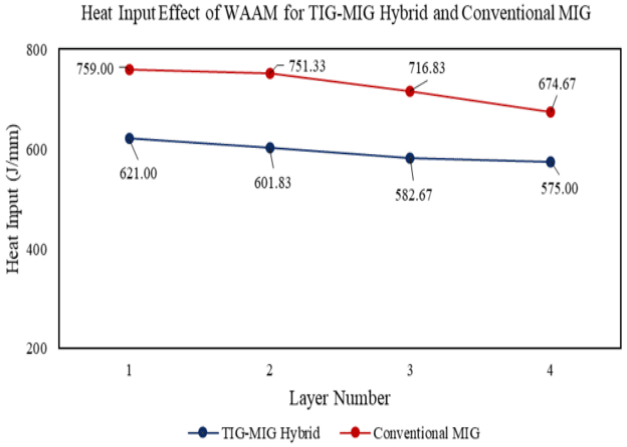

Figure 5: The heat input effect of WAAM for TIG-MIG Hybrid and MIG.

3.2. Thermal analysis of arc striking point and arc extinguishing point for WAAM

Thermal analysis at the arc striking region for both TIG-MIG hybrid and MIG welding in WAAM is presented in Figure 6. The TIG-MIG hybrid weld exhibited approximately, 18.4% increment in heat accumulation (from 195.4 °C to 231.4 °C) as the welding layer increased from the 1st layer to the 4th layer, while MIG showed nearly 10.9% increment (from 221.3 °C to 245.3 °C). This indicates that MIG welding is more prone to excessive heat accumulation, which lead to residual stress (Dinovitzer et al., 2019). Excessive heat accumulation may affect inaccurate weld bead geometry and caused changes in microstructural and mechanical properties as welding layer increased (Karayel & Bozkurt, 2020). After five minutes of interlayer cooling, both processes showed a reduction in temperature at the arc striking point. The TIG-MIG hybrid decreased by 33.5% (from 98.5 °C to 131.5 °C), while MIG decreased by 39.9% (from 99.9 °C to 163.9 °C). These demonstrated that TIG-MIG hybrid welding achieves lower heat input and reduced heat accumulation when compared to MIG, thereby improving thermal management during WAAM.

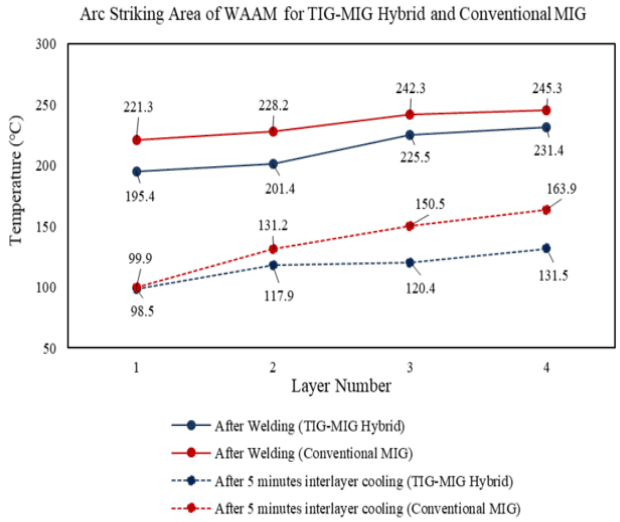

Figure 6: Thermal analysis of TIG-MIG Hybrid and MIG for arc striking area.

Heat accumulation after welding at the arc extinguishing point for TIG-MIG hybrid and MIG increased by 17.9% (from 227.1 °C to 267.8 °C) and by 27.7% (from 253.7 °C to 324.0 °C) respectively (Figure 7). Both welding techniques exhibited higher temperatures at the arc extinguishing point compared to the arc striking point. This is due to the plasma arc's high heat concentration and kinetic energy at the striking point, which melts the filler wire onto the base metal. A dynamic equilibrium of heat radiation and conduction slightly reduces heat concentration. As it approaches the extinguishing point, heat concentration rises again, resulting in higher temperatures (Tang et al., 2019). After five minutes of interlayer cooling, heat accumulation at the arc extinguishing point decreased by 35.3% for the TIG-MIG hybrid (from 92.7 °C to 125.5 °C) and by 44.5% for MIG (from 93.1 °C to 134.5 °C). This reduction is attributed to thermal shock at the arc extinguishing point, where the deposited metal solidifies quickly upon direct contact with ambient temperature, causing abrupt changes in weldment temperature (Liberini et al., 2017).

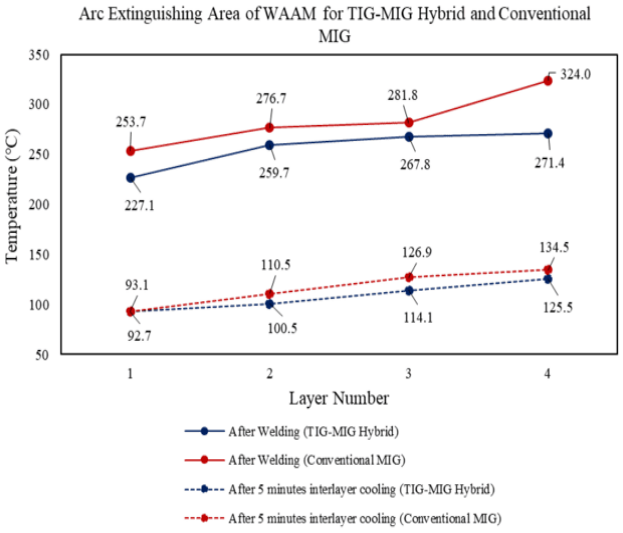

Figure 7: Thermal analysis of TIG-MIG Hybrid and MIG for arc striking area.

3.3 Observation of weld bead geometry for WAAM

3.3.1. Weld bead width of WAAM for TIG-MIG hybrid and MIG

Weld bead width in WAAM increased with layer number for both TIG-MIG hybrid and MIG processes (Figure 8). For the TIG-MIG hybrid, the bead width increased by 33.9% (from 6.190 mm to 8.281 mm), whereas MIG increased about 28.7% (from 6.711 mm to 8.632 mm) as the welding layer deposited from the 1st layer to the 4th layer. Overall, the TIG-MIG hybrid consistently produced narrower bead width compared to MIG. This outcome reflects the influence of the auxiliary TIG arc, which modifies the MIG arc heat distribution and reduces heat input (Chen et al., 2017). According to (Mondal et al., 2016) heat input is directly related to the volume of the weld pool. Lower heat input reduces the molten pool volume and limits the spread of the electrode material across the base metal, resulting in smaller bead width. Contrastingly, MIG welding, with higher heat input, generates a larger weld pool volume and greater spread, producing wider bead width (Shihab et al., 2019).

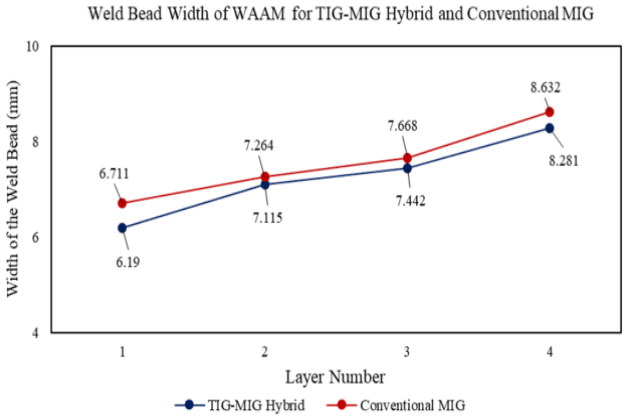

Figure 8: Weld bead width of WAAM for TIG-MIG Hybrid and MIG.

3.3.2. Reinforcement height of WAAM for TIG-MIG hybrid and MIG

The reinforcement height of WAAM increased significantly with layer number for both TIG-MIG hybrid and MIG welding (Figure 9). For the TIG-MIG hybrid, reinforcement height increased by 175.7% (from 2.286 mm to 6.304 mm), while MIG increased approximately, 176.3% (from 2.181 mm to 6.025 mm) as the welding layer deposited from the 1st layer to the 4th layer. Overall, the TIG-MIG hybrid consistently produced higher reinforcement heights compared to that MIG.

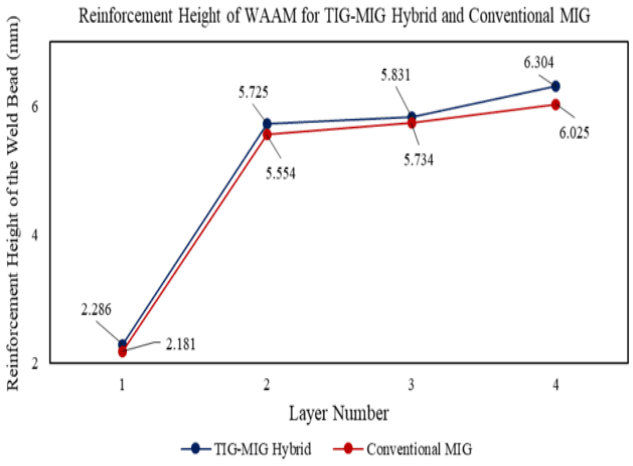

Figure 9: Rinforcement height of WAAM for TIG-MIG Hybrid and MIG.

This suggests the TIG-MIG hybrid, with its lower heat input, generated a smaller molten pool volume and reduced wettability on the base metal, leading to greater reinforcement (Mondal et al., 2016; Roslan et al., 2022). Additionally, the lower current in the TIG-MIG hybrid minimized heat accumulation when compared to MIG, resulting in less melted material per layer and consequently higher reinforcement. Conversely, MIG, with higher heat input, produced more molten material and excessive heat accumulation, which reduced reinforcement height. Thus, lower heat input correlates with narrower bead width but greater reinforcement height, while higher heat input increases bead width but decreases reinforcement height.

3.3.3. Depth penetration of WAAM for TIG-MIG hybrid and MIG

The weld penetration depth in WAAM decreased as the number of layers increased (Figure 10). For the TIG-MIG hybrid, penetration decreased by 36.3% (from 1.281 mm to 0.816 mm), while MIG decreased about 29.6% (from 1.353 mm to 0.952 mm) from the 1st layer to the 4th layer. Overall, the TIG-MIG hybrid consistently produced lower penetration depths compared to MIG, which can be attributed to the auxiliary TIG arc operating at 100 A. The TIG torch acted as the leading source to preheat the base metal, while the MIG

torch trailed to minimize heat concentration, thus reducing the amount of heat transferred into the substrate (Alves de Resende & Scotti, 2017; da Silva Costa & de Resende, 2020). Furthermore, as the welding layer increased, previously deposited molten material accumulated, effectively increasing the standoff distance between the filler wire tip and the base metal surface (Figure 11). This greater standoff distance dispersed the arc, reducing localized heat at the point of contact. Consequently, the heat transferred to the base metal decreased, leading to reduced weld penetration depth (da Silva Costa & de Resende, 2020).

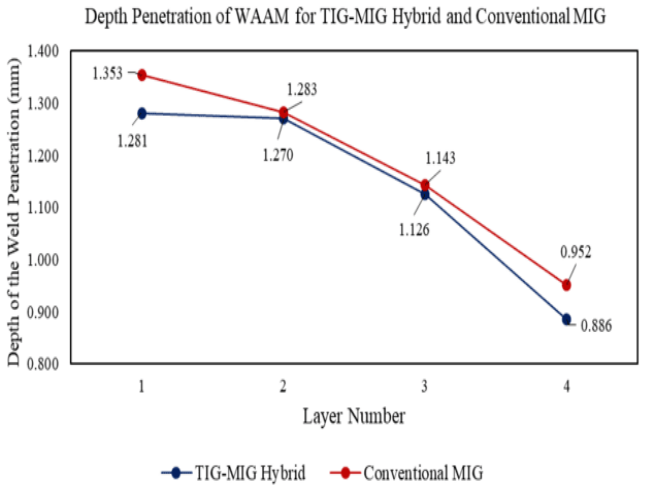

Figure 10: Depth penetration of WAAM for TIG-MIG Hybrid and MIG.

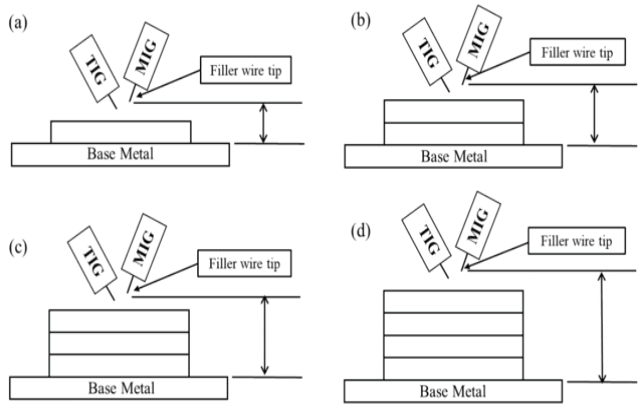

Figure 11: Distance between filler wire tip and base metal as welding layer increases. (a) 1st layer; (b) 2nd layer; (c) 3rd layer; (d) 4th layer

3.4. Microstructure observation of WAAM

Based on the 3% Nital etching in Figure 12, the TIG-MIG hybrid microstructures were characterized by fine and thin dendritic ferrite, whereas MIG exhibited coarse columnar dendrites (Ogundimu et al., 2018). The TIG-MIG hybrid produced microstructures that were approximately 20–25% finer than MIG as the welding layer increased from the 1st layer to the 4th layer. This refinement is attributed to the lower heat input of the hybrid process, which accelerated cooling and promoted finer grain formation. In contrast, the higher heat input of MIG welding slowed the cooling rate, resulting in coarser microstructures (Kumar et al., 2014).

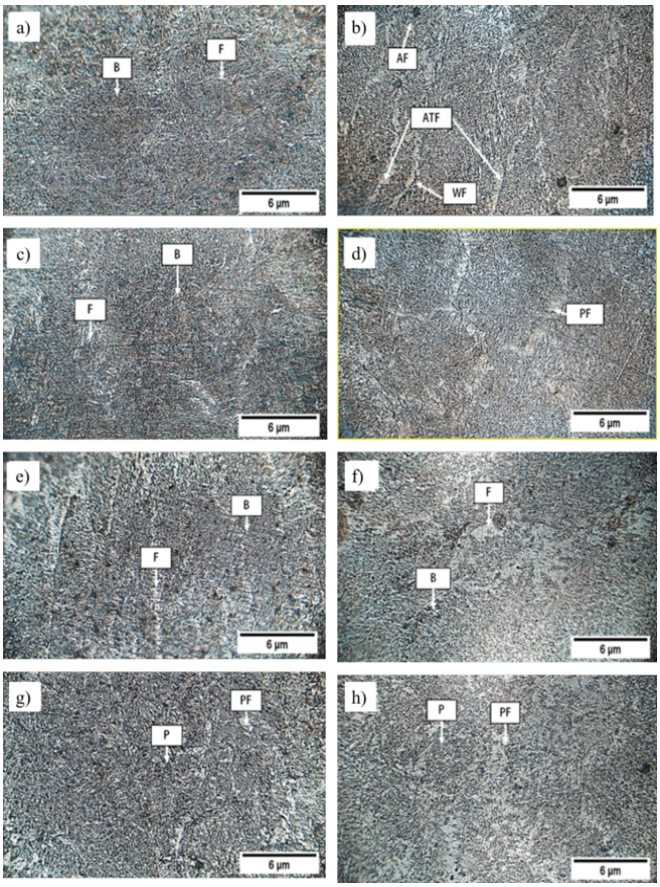

Figure 12: The comparison of TIG-MIG Hybrid (a, c, e, g) and MIG (b, d, f, h) of WAAM by using 3% Nital etchant with different weldment. (a, b) 1st layer; (c, d) 2nd layer; (e, f) 3rd layer; (g, h) 4th layer. Abbreviation: ATF (allotriomorphic ferrite), AF (acicular ferrite) and WF (widmanstatten ferrite), PF (polygonal ferrite), TM (tempered martensite), M (martensite), B (bainite), F (ferrite)

As the welding layer increased from the 2nd layer to the 4th layer, both processes showed microstructural coarsening due to repeated reheating, but the MIG exhibited a 15–20% greater increase in coarseness compared to TIG-MIG hybrid. This was linked to higher thermal shock when the 1st layer was deposited onto the ambient base metal, followed by multiple reheating cycles (Dinovitzer et al., 2019; Liberini et al., 2017). At the 1st layer, TIG-MIG hybrid contained bainite with a small fraction of fine ferrite, indicating a higher cooling rate that increased bainite volume fraction by about 10–15% while reducing ferrite (Chen et al., 2021). However, the MIG had a higher volume fraction of ferrite than the TIG-MIG hybrid at the 1st layer. MIG, however, had ferrite fraction, including allotriomorphic ferrite (ATF), acicular ferrite (AF), and Widmanstatten ferrite (WF) (Wang et al., 2019).

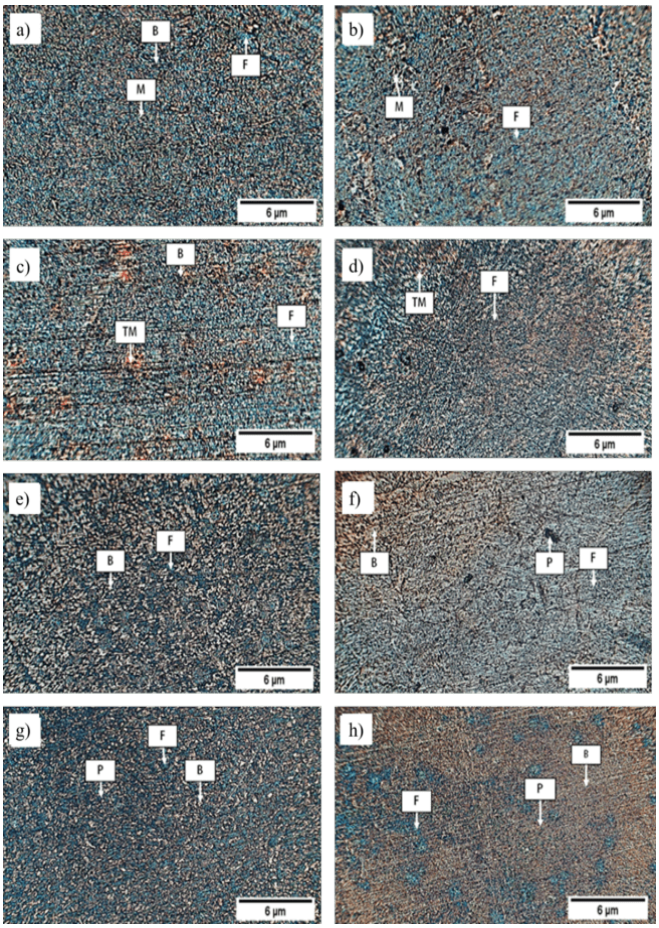

Figure 13: The comparison of TIG-MIG Hybrid (a, c, e, g) and MIG (b, d, f, h) of WAAM by using LePera etchant etchant with different weldment. (a, b) 1st layer; (c, d) 2nd layer; (e, f) 3rd layer; (g, h) 4th layer. Abbreviation: ATF (allotriomorphic ferrite), AF (acicular ferrite) and WF (widmanstatten ferrite), PF (polygonal ferrite), TM (tempered martensite), M (martensite), B (bainite), F (ferrite)

LePera etching revealed that TIG-MIG hybrid observed bainite (black) and ferrite (blue), while MIG revealed predominantly ferrite (Figure 13). Both processes exhibited martensite (beige), formed due to thermal shock when contacted with ambient temperature, with MIG showing a higher martensite fraction (~10% more) than TIG-MIG hybrid (Dobras & Rutkowska-Gorczyca, 2018). At the 2nd layer, TIG-MIG hybrid displayed ferrite and bainite, while MIG formed polygonal ferrite (PF) (Zhou et al., 2017), reflecting its higher heat input and slower cooling. Both processes also showed tempered martensite (TM), but TIG-MIG hybrid produced ~15% less carbide precipitation due to lower heat accumulation (Dinovitzer et al., 2019; Grosch, 2015). By the 3rd and 4th layers, TIG-MIG hybrid microstructures remained dominated by ferrite and bainite, while MIG exhibited ferrite (blue), pearlite (black), and bainite (brown), with bainite regions being ~20% larger than in TIG-MIG hybrid. This indicates that MIG, with higher heat input, promoted more low-temperature microstructures, whereas TIG-MIG hybrid's auxiliary TIG arc preheated the previous layer, reducing solidification stresses and refining the weld structure (Chen et al., 2017).

3.5. Microhardness analysis of WAAM for TIG-MIG Hybrid and MIG of WAAM

Based on the overall experimental results in Figure 14, the TIG-MIG hybrid exhibited lower hardness values than MIG as the welding layer increased. The average hardness of TIG-MIG hybrid samples decreased by 41.4% (from 221.57 HV to 129.9 HV), while MIG decreased by 31.4% (from 245.17 HV to 168.17 HV). This decreasing trend reflects the lower heat input and preheating effect of the TIG torch in the hybrid process, which refined the microstructure (Rodrigues et al., 2019). The hardness of welded samples is strongly dependent on microstructure formation, following the order: martensite (M) > tempered martensite (TM) > bainite (B) > pearlite (P) > ferrite (F) (Mohan & Gopi, 2020). At the 1st welding layer, the average hardness of TIG-MIG hybrid was already lower than MIG, which can be explained by the TIG arc preheating the base metal and reducing solidification, thereby minimizing martensite formation (Ogundimu et al., 2018).

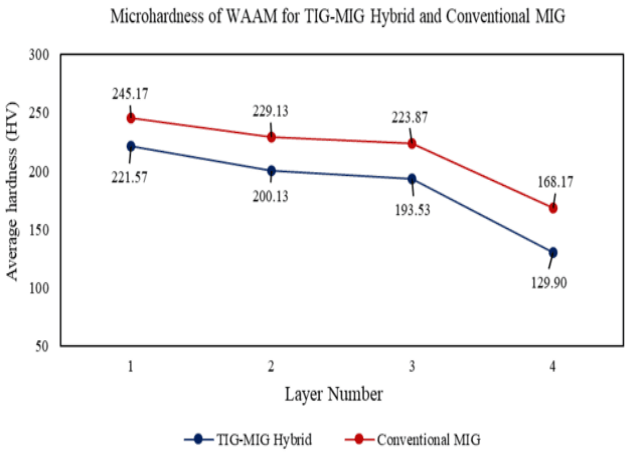

Figure 14: The microhardness of WAAM for TIG-MIG Hybrid and MIG.

As the welding layer increased, hardness continued to decrease. This is because the 1st layer experienced lower temperatures and better heat dissipation, promoting finer microstructures. However, from the 2nd to the 4th layer, heat accumulation increased, leading to coarser microstructures due to poor heat dissipation and repeated thermal cycling. Consequently, smaller grains at the lower layers exhibited higher hardness due to more grain boundaries for dislocation, while larger grains at higher layers resulted in lower hardness values (Zuo et al., 2018).

4. CONCLUSION

TIG-MIG hybrid demonstrated more stable metal transfer compared to MIG, as the repulsion effects of

electromagnetic forces on the molten metal were reduced, minimizing spatter generation. The TIG-MIG hybrid reduced heat input by approximately 7.41% (from 621.00 J/mm to 575.00 J/mm) as the welding layer increased, aided by the TIG arc preheating effect that minimized heat losses. Heat accumulation at the arc striking region was lower in TIG-MIG hybrid (an increase of 18.4%) compared to MIG (an increase of 10.9%) as the welding layer progressed from the 1st to the 4th layer, confirming the hybrid's ability to better manage thermal gradients. Weld bead geometry showed that TIG-MIG hybrid produced higher reinforcement height (increased by 175.7%) compared to MIG (176.3%), while penetration depth and hardness values decreased in both processes. However, the differences between TIG-MIG hybrid and MIG in terms of penetration and hardness were relatively small overall. Microstructural observations revealed that TIG-MIG hybrid produced finer dendritic ferrite compared to the coarser columnar structures of MIG, indicating refinement due to lower heat input. Although TIG-MIG hybrid exhibited slightly lower hardness than MIG, the overall differences in hardness, penetration, and other mechanical properties were not substantial. This suggests that while TIG-MIG hybrid offers advantages in heat input control and microstructural refinement, the improvements in mechanical performance compared to MIG are modest.

REFERENCES

Alves de Resende, A., & Scotti, A. (2017). Influence of current levels, the tilt angle of the torch and the distance between the torch and the part on the geometry of the weld bead using 'Plasma-MIG'with concentric arcs. *Welding international, 31*(10), 747-757. https://doi.org/https://doi.org/10.1080/09507116.2016.1218628

Bach, T. T., Hung, L. Q., Phong, P. T., Hieu, N. M., Le, X. H., Damian, D., & Nguyen, V. A. (2025). Wire Arc Additive Manufacturing: A Review on Technology, Challenges, and Applications. International Conference on Sustainability and Emerging Technologies for Smart Manufacturing,

Chen, J., Zong, R., Wu, C., Padhy, G. K., & Hu, Q. (2017). Influence of low current auxiliary TIG arc on high speed TIG-MIG hybrid welding. *Journal of Materials Processing Technology, 243*, 131-142. https://doi.org/https://doi.org/10.1016/j.jmatprotec.2016.12.012

Chen, S., Li, L., Peng, Z., Huo, X., & Gao, J. (2021). Microstructure evolution during continuous cooling process in Ti microalloyed steel. Journal of Physics: Conference Series,

da Silva Costa, G. C., & de Resende, A. A. (2020). Evaluation of the TIG–MIG/MAG welding process in direct polarity. *SN Applied Sciences, 2*(2), 164. https://doi.org/https://doi.org/10.1007/s42452-020-1953-7

Ding, D., Pan, Z., Cuiuri, D., & Li, H. (2015). Wire-feed additive manufacturing of metal components: technologies, developments and future interests. *The International Journal of Advanced Manufacturing Technology, 81*(1), 465-481. https://doi.org/https://doi.org/10.1007/s00170-015-7077-3

Dinovitzer, M., Chen, X., Laliberte, J., Huang, X., & Frei, H. (2019). Effect of wire and arc additive manufacturing (WAAM) process parameters on bead geometry and microstructure. *Additive Manufacturing, 26*, 138-146. https://doi.org/https://doi.org/10.1016/j.addma.2018.12.013

Dobras, D., & Rutkowska-Gorczyca, M. (2018). Application of color etching to study the microstructure of TRIP steel after laser remelting. *Welding Technology Review, 90*. https://doi.org/https://doi.org/10.26628/wtr.v90i12.984

Grosch, J. (2015). Fatigue resistance of carburized and nitrided steels. In *Thermochemical Surface Engineering of Steels* (pp. 209-240). Elsevier. https://doi.org/https://doi.org/10.1533/9780857096524.2.209

He, Y., Song, X., Yang, Z., Duan, R., Xu, J., Wang, W., Chen, L., Shi, M., & Chen, S. (2025). Research and Development Progress of Laser–Arc Hybrid Welding: A Review. *Metals, 15*(3), 326. https://doi.org/https://doi.org/10.3390/met15030326

Jafari, D., Vaneker, T. H., & Gibson, I. (2021). Wire and arc additive manufacturing: Opportunities and challenges to control the quality and accuracy of manufactured parts. *Materials & Design, 202*, 109471. https://doi.org/https://doi.org/10.1016/j.matdes.2021.109471

Jamian, S., Kamarudin, K. A., Nor, M. K. M., Ibrahim, M. N., & Choiron, M. A. (2018). An overview of fracture mechanics with ANSYS. *International Journal of Integrated Engineering, 10*(5). https://doi.org/https://doi.org/10.30880/ijie.2018.10.05.010

Kapil, S., Rajput, A. S., & Sarma, R. (2022). Hybridization in wire arc additive manufacturing. *Frontiers in Mechanical Engineering, 8*, 981846. https://doi.org/https://doi.org/10.3389/fmech.2022.981846

Karayel, E., & Bozkurt, Y. (2020). Additive manufacturing method and different welding applications. *Journal of Materials Research and Technology, 9*(5),11424-11438. https://doi.org/https://doi.org/10.1016/j.jmrt.2020.08.039

Kumar, R., Arya, H. K., & Saxena, R. (2014). Experimental determination of cooling rate and its effect on microhardness in submerged arc welding of mild steel plate (grade c-25 as per IS 1570). *J Mater Sci Eng, 3*(2), 1-4. https://doi.org/https://doi.org/10.4172/2169-0022.1000138

Liberini, M., Astarita, A., Campatelli, G., Scippa, A., Montevecchi, F., Venturini, G., Durante, M., Boccarusso, L., Minutolo, F. M. C., & Squillace, A. (2017). Selection of optimal process parameters for wire arc additive manufacturing. *Procedia Cirp, 62*, 470-474. https://doi.org/https://doi.org/10.1016/j.procir.2016.06.124

Mohan, D. G., & Gopi, S. (2020). Induction assisted friction stir welding: a review. *Australian Journal of Mechanical Engineering*. https://doi.org/https://doi.org/10.1080/14484846.2018.1432089

Mondal, A., Kumar Saha, M., Hazra, R., & Das, S. (2016). Influence of heat input on weld bead geometry using duplex stainless steel wire electrode on low alloy steel specimens. *Cogent Engineering, 3*(1), 1143598. https://doi.org/https://doi.org/10.1080/23311916.2016.1143598

Ogundimu, E. O., Akinlabi, E. T., & Erinosho, M. F. (2018). Study on microstructure and mechanical properties of 304 stainless steel joints by TIG–MIG hybrid welding. *Surface Review and Letters, 25*(01), 1850042. https://doi.org/https://doi.org/10.1142/S0218625X18500427

Oliveira, J., Santos, T., & Miranda, R. (2020). Revisiting fundamental welding concepts to improve additive manufacturing: From theory to practice. *Progress in Materials Science, 107*, 100590. https://doi.org/https://doi.org/10.1016/j.pmatsci.2019.100590

Rodrigues, T. A., Duarte, V., Miranda, R. M., Santos, T. G., & Oliveira, J. P. (2019). Current status and perspectives on wire and arc additive manufacturing (WAAM). *Materials, 12*(7), 1121. https://doi.org/https://doi.org/10.3390/ma12071121

Roslan, R. A. E., Mamat, S., Teo, P. T., Mohamad, F., Toshifumi, Y., Tashiro, S., & Tanaka, M. (2022). Numerical simulation of arc behaviour in TIG/MIG hybrid welding process of aluminium alloy. AIP Conference Proceedings,

Shah, A., Aliyev, R., Zeidler, H., & Krinke, S. (2023). A review of the recent developments and challenges in wire arc additive manufacturing (WAAM) process. *Journal of Manufacturing and Materials Processing, 7*(3), 97. https://doi.org/https://doi.org/10.3390/jmmp7030097

Shihab, S. K., Mohamed, R. H., & Mubarek, E. M. (2019). Optimization of process parameters in cladding of stainless steel over mild steel. *Materials Today: Proceedings, 16*, 816-823. https://doi.org/https://doi.org/10.1016/j.matpr.2019.05.163

Singh, N., Hameed, P., Ummethala, R., Manivasagam, G., Prashanth, K., & Eckert, J. (2020). Selective laser manufacturing of Ti-based alloys and composites: impact of process parameters, application trends, and future prospects. *Materials today advances, 8*, 100097. https://doi.org/https://doi.org/10.1016/j.mtadv.2020.100097

Snopiński, P., Krol, M., Tański, T., & Krupińska, B. (2018). Effect of cooling rate on microstructural development in alloy ALMG9. *Journal of Thermal Analysis and Calorimetry, 133*(1), 379-390. https://doi.org/https://doi.org/10.1007/s10973-018-7313-9

Tang, S., Wang, G., Huang, C., & Zhang, H. (2019). Investigation and control of weld bead at both ends in WAAM. https://doi.org/http://dx.doi.org/10.26153/tsw/17307

Wang, C., Wang, X., Kang, J., Yuan, G., & Wang, G. (2019). Effect of thermomechanical treatment on acicular ferrite formation in Ti–Ca deoxidized low carbon steel. *Metals, 9*(3), 296. https://doi.org/https://doi.org/10.3390/met9030296

Yang, D., He, C., & Zhang, G. (2016). Forming characteristics of thin-wall steel parts by double electrode GMAW based additive manufacturing. *Journal of Materials Processing Technology, 227*, 153-160. https://doi.org/https://doi.org/10.1016/j.jmatprotec.2015.08.021

Yang, D., Wang, G., & Zhang, G. (2017). A comparative study of GMAW-and DE-GMAW-based additive manufacturing techniques: thermal behavior of the deposition process for thin-walled parts. *The International Journal of*

Advanced Manufacturing Technology, 91(5), 2175-2184. https://doi.org/https://doi.org/10.1007/s00170-016-9898-0

Zhang, Y., Wu, L., Guo, X., Kane, S., Deng, Y., Jung, Y.-G., Lee, J.-H., & Zhang, J. (2018). Additive manufacturing of metallic materials: a review. *Journal of Materials Engineering and Performance, 27*(1), 1-13. https://doi.org/https://doi.org/10.1007/s11665-017-2747-y

Zhou, X., Dong, J., Liu, Y., Liu, C., Yu, L., Huang, Y., & Li, H. (2017). Austenite to polygonal-ferrite transformation and carbide precipitation in high strength low alloy steel. *International Journal of Materials Research, 108*(1), 12-19. https://doi.org/https://doi.org/10.3139/146.111454

Zuo, W., Ma, L., Lu, Y., Li, S.-y., Ji, Z., & Ding, M. (2018). Effects of solution treatment temperatures on microstructure and mechanical properties of TIG–MIG hybrid arc additive manufactured 5356 aluminum alloy. *Metals and Materials International, 24*(6), 1346-1358. https://doi.org/https://doi.org/10.1007/s12540-018-0142-3

